High Sensitivity of Arctic Liquid Clouds to Long-Range Anthropogenic Aerosol Transport

Quentin Coopman, T. J. Garrett, D. Finch, J. Riedi

AGU PUBLICATIONS

Geophysical Research Letters

RESEARCH LETTER
10.1002/2017GL075795

Key Points:
- Arctic liquid clouds are particularly sensitive to anthropogenic pollution from lower latitudes
- Biomass burning has a weaker impact compared to aerosol arriving from anthropogenic sources
- Analyses of interactions between pollution and clouds must account for local meteorological variability

Supporting Information:
- Supporting Information S1
- Figure S1
- Figure S2
- Movie S1

Correspondence to:
Q. Coopman,
quentin.coopman@kit.edu

Citation:
Coopman, Q., Garrett, T. J., Finch, D. P., & Riedi, J. (2018). High sensitivity of arctic liquid clouds to long-range anthropogenic aerosol transport. *Geophysical Research Letters*, *45*, 372–381. https://doi.org/10.1002/2017GL075795

Received 28 SEP 2017
Accepted 5 NOV 2017
Accepted article online 9 NOV 2017
Published online 3 JAN 2018

High Sensitivity of Arctic Liquid Clouds to Long-Range Anthropogenic Aerosol Transport

Q. Coopman[1,2,3], T. J. Garrett[2], D. P. Finch[4], and J. Riedi[1]

[1]Univ. Lille, CNRS, UMR 8518 - LOA - Laboratoire d'Optique Atmosphérique, Lille, France, [2]Department of Atmospheric Sciences, University of Utah, Salt Lake City, UT, USA, [3]Now at Institute of Meteorology and Climate Research, Karlsruhe Institute of Technology, Karlsruhe, Germany, [4]School of Geoscience, University of Edinburgh, Edinburgh, UK

Abstract The rate of warming in the Arctic depends upon the response of low-level microphysical and radiative cloud properties to aerosols advected from distant anthropogenic and biomass-burning sources. Cloud droplet cross-section density increases with higher concentrations of cloud condensation nuclei, leading to an increase of cloud droplet absorption and scattering radiative cross sections. The challenge of assessing the magnitude of the effect has been decoupling the aerosol impacts on clouds from how clouds change solely due to natural meteorological variability. Here we address this issue with large, multi-year satellite, meteorological, and tracer transport model data sets to show that the response of low-level clouds in the Arctic to anthropogenic aerosols lies close to a theoretical maximum and is between 2 and 8 times higher than has been observed elsewhere. However, a previously described response of arctic clouds to biomass-burning plumes appears to be overstated because the interactions are rare and modification of cloud radiative properties appears better explained by coincident changes in temperature, humidity, and atmospheric stability.

1. Introduction

Increased concentrations of cloud condensation nuclei (CCN) cause cloud droplets to become more numerous, and for constant liquid water content, this leads to smaller droplets and higher radiative cross-section densities. The radiative impacts of CCN are important enough to potentially lead to a warmer surface and accelerated melting of arctic sea ice (Garrett & Zhao, 2006), particularly in winter and spring when the longwave response dominates and pollution levels are high (Zhao & Garrett, 2015). The last decade has seen a lengthening and intensification of boreal forest fires that has led to increased biomass-burning (BB) aerosol concentrations in the Arctic, a trend that is expected to continue (Flannigan et al., 2009). On the other hand, a downward trend in midlatitude anthropogenic (ANT) emissions has lowered concentrations of arctic sulfur (Hirdman et al., 2010) although this may be offset by future Arctic industrialization (Lindholt & Glomsrød, 2012) and shipping (Pizzolato et al., 2014).

Assessment of the impact of these aerosol changes on arctic clouds has been a challenge because surface and airborne observations in the Arctic are sparse (Earle et al., 2011; Garrett & Zhao, 2006), aerosol compositions are regionally varied and complex, and both aerosol transport and cloud formation are determined by meteorological conditions (Stohl, 2006), in particular by the humidity, temperature, and lower tropospheric stability (LTS) (Andersen & Cermak, 2015; Cox et al., 2015; Klein & Hartmann, 1993).

Our study aims to robustly isolate how lower latitude ANT and BB aerosols affect clouds over the Arctic, independent of local meteorological changes (Stevens & Feingold, 2009). For maximum coverage, we use space-based data sets for the retrieval of low-level liquid cloud properties, and we quantify the magnitude of aerosol-cloud interactions (ACI) by vertically and horizontally colocating clouds with pollution concentrations from numerical tracer transport model output for the Arctic for a period between March and September for the years 2005 to 2010.

2. Methods

The ACI parameter has previously been introduced as the ratio of relative changes in cloud optical depth τ and cloud droplet effective radius r_e to relative changes in local CCN concentrations (Feingold et al., 2001).

For the purpose of calculating ACI, space-based data sets have often been used as they offer the advantage of wide temporal and spatial coverage (McComiskey & Feingold, 2012).

The primary drawback of many prior space-based ACI calculations is that clouds are nearly opaque, making it infeasible to retrieve aerosol concentrations and cloud properties for the same location and meteorological conditions (Bréon et al., 2002). Further, aerosols affect cloud properties, including precipitation rates, and thereby can affect their own concentrations. The difficulty of relating aerosols to clouds when neither is independent of the other can be avoided by using a passive tracer of pollution plumes as an aerosol proxy. Carbon monoxide (CO) is a particularly good candidate as, like aerosols from biomass-burning and fossil fuel sources, it is a product of incomplete combustion. CO and aerosols tend to correlate well close to industrial sources in nonprecipitating air parcels (Garrett & Zhao, 2006; Longley et al., 2005). Further, CO emitted by large forest fires is highly correlated with aerosols in arctic pollution plumes (Paris et al., 2009; Stohl et al., 2007; Warneke et al., 2009, 2010). CO has been used previously as an aerosol proxy for in situ studies of aerosol-cloud interactions (Garrett et al., 2006, 2010; Yang et al., 2015; Zamora et al., 2016) as well as those employing satellite data sets (Avey et al., 2007; Brioude et al., 2009; Coopman et al., 2016; Tietze et al., 2011).

Of course, CO by itself does not interact with clouds, but its utility for studies of aerosol-cloud interactions is that it serves as an indicator of the presence of polluted air that is possibly loaded with aerosols (Garrett et al., 2006). Both CCN and CO are equally diluted along transport pathways, so the modeled spatial and temporal distributions of the two pollutants should generally be expected to correlate further downwind provided that CO is modeled as being purely passive and not subject to any sources or sinks. Zamora et al. (2016) calculated the ACI parameter from aircraft measurements of arctic clouds interacting with biomass-burning plumes. Their results were generally consistent whether CCN or CO was used to obtain ACI.

In the present study, we use CO concentrations from a tracer transport model as a proxy for aerosol concentrations, accounting for the possibility that aerosols have previously been scavenged from the atmosphere during long-range transport. We derive a net ACI (ACI^{net}) parameter based upon ensembles of space-based retrievals of cloud properties that are temporally, vertically, and horizontally colocated with concentrations of tracer transport model output of carbon monoxide χ_{CO}, where CO is set as a purely passive, chemically nonreactive species (Coopman et al., 2016). Thus,

$$ACI^{net}_{r_e} = -\frac{d \ln r_e}{d \ln \chi_{CO}} \tag{1}$$

$$ACI^{net}_{\tau} = \frac{d \ln \tau}{d \ln \chi_{CO}}. \tag{2}$$

Considering a CO pollution tracer focuses the study on aerosols from combustion sources only. Other types of aerosols, such as desert dust, are not considered.

This approach is shown in Figure 1. If there is no precipitation en route to the Arctic, then ACI^{net} is determined solely by the local efficiency with which increased aerosol concentrations perturb cloud properties. Expected values range from 0 to a theoretical maximum that is close to 0.33 assuming a one to one correspondence between CCN and droplet number concentration for a fixed cloud liquid water path (LWP) (McComiskey et al., 2009). Where there has been precipitation during pollution plume transport, however, aerosols can be washed from the atmosphere, leaving the passive modeled CO tracer behind. In this case, the ACI^{net} value will tend toward zero, even if the aerosols were previously efficient CCN (Garrett et al., 2011). By accounting for both aerosol removal and CCN efficiency, using ACI^{net} extends the purely local sensitivities implied by the more traditional ACI to a more global sensitivity: It confers a particularly powerful method for assessing the potential of distant midlatitude pollution sources to modify cloud properties in the remote Arctic (Coopman et al., 2016).

3. Data

Cloud microphysical parameters are retrieved from a combination of two instruments that are part of the A-train mission (Stephens et al., 2002): POLDER-3 (POLarization and Directionality of the Earth's Reflectances) (Bréon & Colzy, 1999) on the PARASOL (Polarization and Anisotropy of Reflectances for Atmospheric Sciences coupled with Observations from a Lidar) platform and Level-2 Collection 6 data set (Baum et al., 2012; King et al., 2006) from MODIS (Moderate Resolution Imaging Spectroradiometer) (Platnick et al., 2003) on board

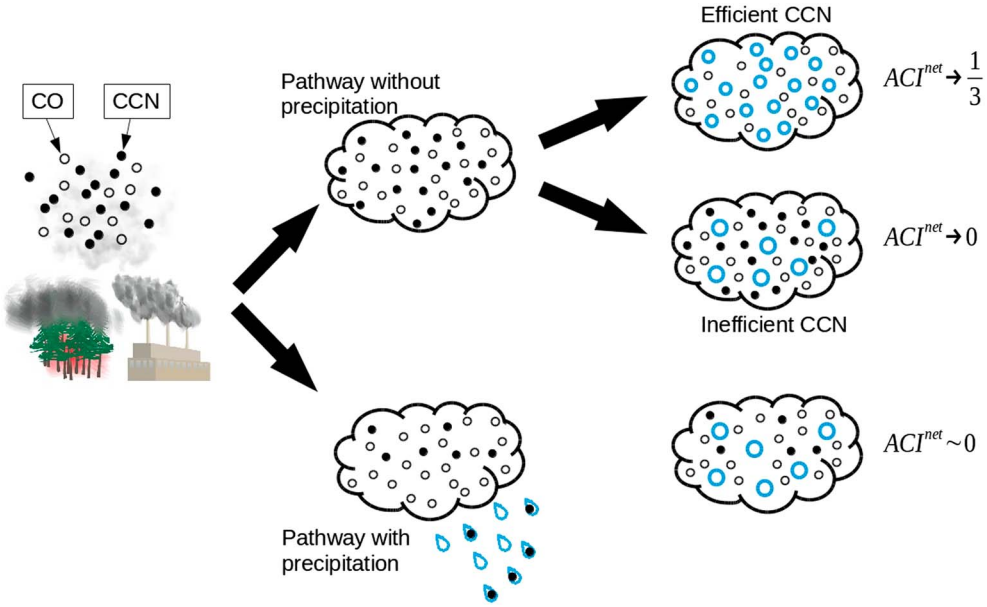

Figure 1. The relationship between a passive CO tracer in a tracer transport model and aerosol concentrations along differing long-range transport pathways. CO and aerosols are correlated at the source region. Depending on the efficiency of aerosols to act as CCN and the occurrence of precipitation during transport, the impact of distant pollution plumes on arctic clouds defined by ACI^{net} (equations (1) and (2)) varies between 0 and 1/3.

the Aqua satellite. Cloud top pressure from POLDER-3 is derived from oxygen A-Band absorption above cloud. Especially in the Arctic, it acts as a better proxy for low-level cloud than MODIS cloud top pressure derived from the cloud emission temperature (Buriez et al., 1997). An algorithm that uses shortwave, thermal infrared, and visible measurements from MODIS and multiangle polarization measurements from POLDER-3 provides a phase index ranging from 0 for liquid clouds to 200 for ice clouds within each cloud pixel (Riedi et al., 2010). Coopman et al. (2016) showed that the distribution of this phase index over the Arctic can be divided into three distinct modes with thresholds at 0 and 60, 60 and 140, and 140 and 200, assumed to correspond, respectively, to liquid, unknown, and ice phase clouds (Riedi et al., 2010).

To evaluate changes in cloud microphysical parameters due to the presence of pollution plumes, we use as a passive tracer of aerosols χ_{CO} from GEOS-Chem v9-01-03 (Bey et al., 2001). The model considers three CO sources: (i) fossil fuel emissions from the Emissions Database for Global Atmospheric Research, European Monitoring and Evaluation Programme, Big Bend Regional Aerosol and Visibility Observationa, and STREETS; (ii) BB emissions from the Global Fire Emission Data Set ; and iii) biogenic emissions from the Model of Emissions of Gases and Aerosol from Nature (MEGAN) data set. The model is run at a spatial resolution of 2° in latitude and 2.5° in longitude at 47 native vertical levels to track concentrations of pollution downwind of source regions. The model is extensively described in Parrington et al. (2012) and Finch et al. (2014). For a more detailed discussion on model capabilities (Bey et al., 2001; Finch et al., 2014; Fisher et al., 2010; Mackie et al., 2016; Parrington et al., 2012) and model evaluation with arctic ground-based measurements, see the supporting information Text S1, Table S1, and Figure S1.

To ensure that changes in cloud microphysical properties are due to pollution plumes and not to specific meteorological parameters, we control for specific humidity (SH), LTS, cloud top temperature (T_C), and LWP. LWP and T_C are retrieved using satellite measurements and LTS and SH are obtained from the ERA-Interim (ERA-I) reanalysis data set from ECMWF (European Centre for Medium-Range Weather Forecasts) (Berrisford et al., 2011). ERA-I provides meteorological values at 60 different pressure levels with a spatial resolution of 1.5° × 1.5°. Temperature contrasts between land and ocean can be significant, and surface fluxes from these two surface types are treated differently within the ERA-I interpolation scheme (Dee et al., 2011). To avoid a potential bias, we limit our analyses to grid cells that are exclusively oceanic. The reanalysis provides SH and temperature at several pressure levels. We use SH at 700 hPa as a proxy of lower atmosphere humidity and LTS is defined by the difference in potential temperature between 700 hPa and 1000 hPa (Klein & Hartmann, 1993).

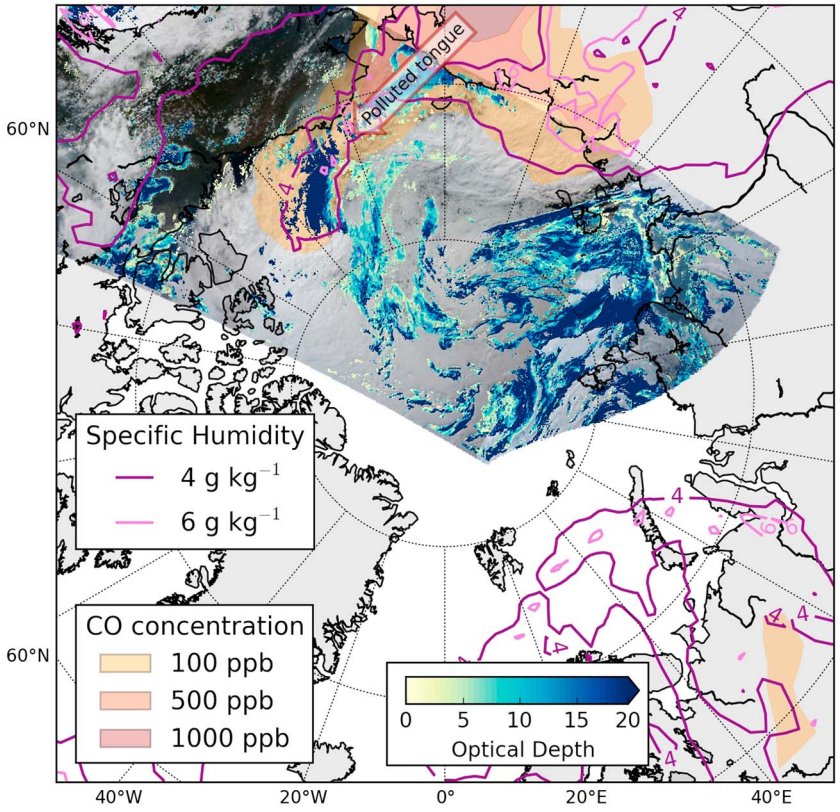

Figure 2. Low-level τ, SH at 700 hPa, and χ_{CO} of the first 3 km on 31 July at 21:30 UTC. The SH and the χ_{CO} are, respectively, retrieved by ERA-Interim reanalysis and GEOS-Chem and they are both showing by the contour plots. Values of τ are retrieved by the instrument Aqua on MODIS platform satellite.

Because satellite, tracer transport model, and reanalysis data sets use different grids, each is projected onto an equal-area sinusoidal grid where the resolution at the equator is 54 km × 54 km, or 2916 km^2. CO tracer concentrations from the numerical model are averaged between two temporal points with a resolution of 3 h. CO concentration pixels are spatially and temporally colocated with each satellite-retrieval pixel. ERA-I reanalyses have a temporal resolution of 6 h. To match the times of the meteorological parameters with the numerical CO output, we linearly interpolate between nearest neighbors in the reanalysis data. We consider only oceanic clouds lower than 3 km with latitudes higher than 65° .

4. Results and Discussions

To illustrate the importance of isolating meteorological state for assessments of the magnitude of ACI^{net}, Figure 2 shows a BB event on 31 July 2010 at 2130 UTC where a BB plume from northeastern Siberia with high SH and high χ_{CO} was advected to the Beaufort Sea region. From the shapes and locations of the 4 g kg^{-1} SH and the 100 ppb χ_{CO} isolines it is clear that the two properties covary. Because clouds were also present in the polluted tongue, the implication is that any observed change in cloud τ could mistakenly be attributed to higher pollution levels when they would be more reasonably explained by increased moisture. See Movie S1 from the supporting information for an animation of the entire day.

Extracting the potential impact of pollution plumes on clouds from meteorological noise requires large data sets. From 2005 to 2010, low-level arctic cloud properties remotely sensed by POLDER and MODIS are colocated with χ_{CO} from GEOS-Chem.

Out of the 10,119,668 grid cells with colocated cloud and CO data, 3,777,125 grid cells are associated with ANT plumes, and 37,732 grid cells are associated with BB plumes, representing, respectively, 37% and 0.4% of the cloudy data set summarized in Table 1. The relative fraction of BB pollution to total pollution is used to divide the data into five quintiles: a fraction below 0.2 nominally identifies ANT-dominated aerosol regimes whereas a ratio greater than 0.8 indicates a BB-dominated aerosol regime. BB aerosol regimes have median

Table 1
Meteorological Parameters Associated With ANT and BB Aerosol Regimes

	ANT plumes	BB plumes	Entire data set
SH (g kg^{-1})	1.9	5.1	2.5
LTS (K)	17.7	23.8	18.7
T_C (°C)	−8.4	0.4	−4.4
No. of grid cell	3,777,125	37,732	10,119,668

Note. For colocated cloud and CO grid cells, median values of specific humidity (SH), lower tropospheric stability (LTS), cloud top temperature (T_C) for BB and ANT aerosol regimes and for all grid cells.

values of SH, LTS, and T_C that are, respectively, 5.1 g kg^{-1}, 23.8 K, and 0.4°C, whereas ANT regimes have median values of 1.9 g kg^{-1}, 17.7 K, and −8.4°C. For comparison, the entire data set has median values of 2.6 g kg^{-1}, 18.7 K, and −4.4°C. Therefore, cloudy air dominated by BB aerosols tends to be warmer, moister, and more stable than typical air parcels dominated by ANT aerosol regimes. For the period between March and September where coincident satellite and tracer transport model output are available, χ_{CO} in BB plumes are a minimum in March and a maximum in August. By contrast, χ_{CO} from ANT plumes are a minimum in August and a maximum in March. Notably, interactions between BB plumes and clouds are nearly one hundred times rarer than interactions between ANT plumes and clouds. A possible reason is that BB events tend to occur when temperatures are high and the humidity low, conditions that are generally unfavorable for cloud formation (Monks et al., 2012).

Clean and polluted pollution regimes tend to be associated with different meteorological states. Figure 3 shows the data sorted according to polluted and clean aerosol regimes defined by the upper and lower quartiles in χ_{CO}. Levene statistical tests applied to SH, LTS, and T_C indicate that to within a 95% confidence interval, clean and polluted air parcels dominated by both ANT and BB aerosol regimes are statistically distinct (Levene values >30 in each case) implying that BB and ANT plumes tend to occur during different weather conditions. Median values of SH, LTS, and T_C in polluted BB plumes are, respectively, 4.5 g kg^{-1}, 23.1 K, and −0.5 °C compared to 6.4 g kg^{-1}, 26.9 K, and 1.6 °C in clean BB plumes. Median values of SH, LTS, and T_C in polluted ANT plumes are, respectively, 3.0 g kg^{-1}, 19.6 K, and −3.4 °C compared to 1.3 g kg^{-1}, 17.0 K, and −12.3 °C in clean

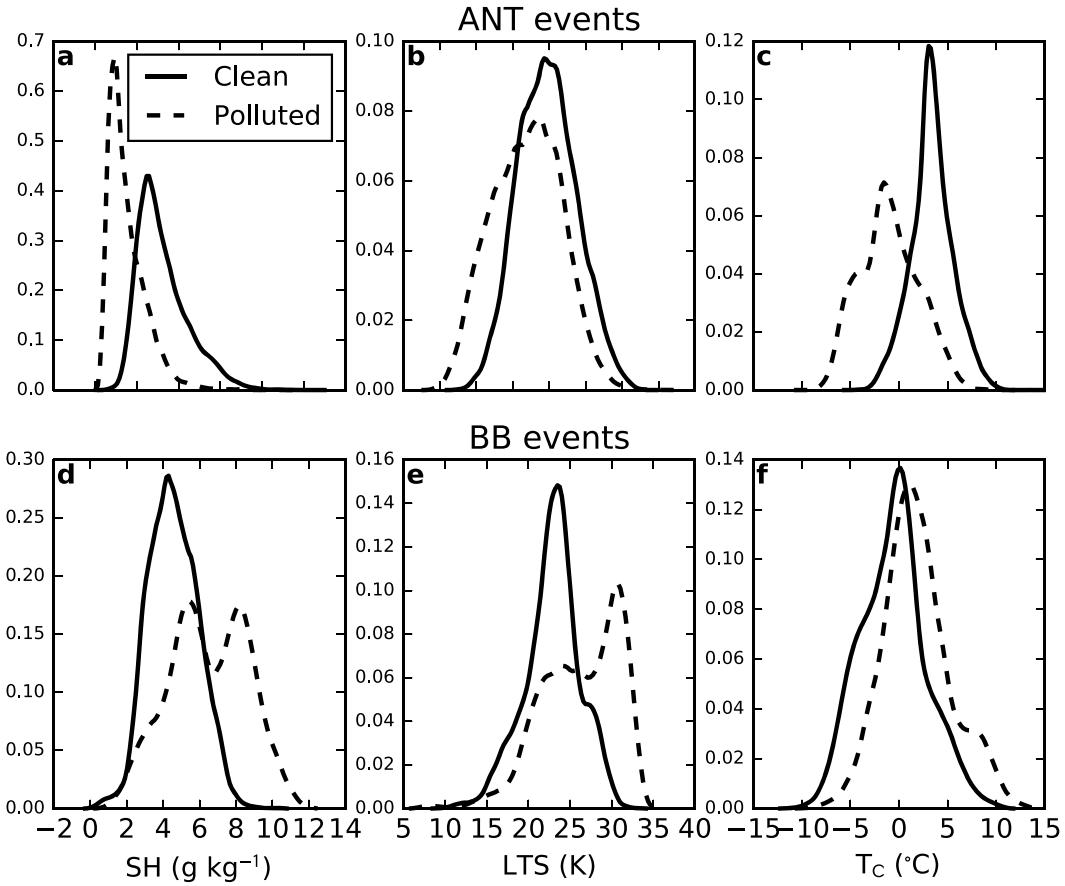

Figure 3. Normalized probability density function of (a, d) SH, (b, e) LTS, and (c, f) T_C for clean and polluted air parcels during ANT (Figures 3a–3c) and BB aerosol regimes (Figures 3d–3f). Clean and polluted BB air parcels corresponding to the lower and upper quartiles in CO concentration have values of χ_{CO} less than 155 ppb and greater than 262 ppb, respectively. Clean and polluted ANT air parcels have values of χ_{CO} less than 54 ppb and greater than 82 ppb.

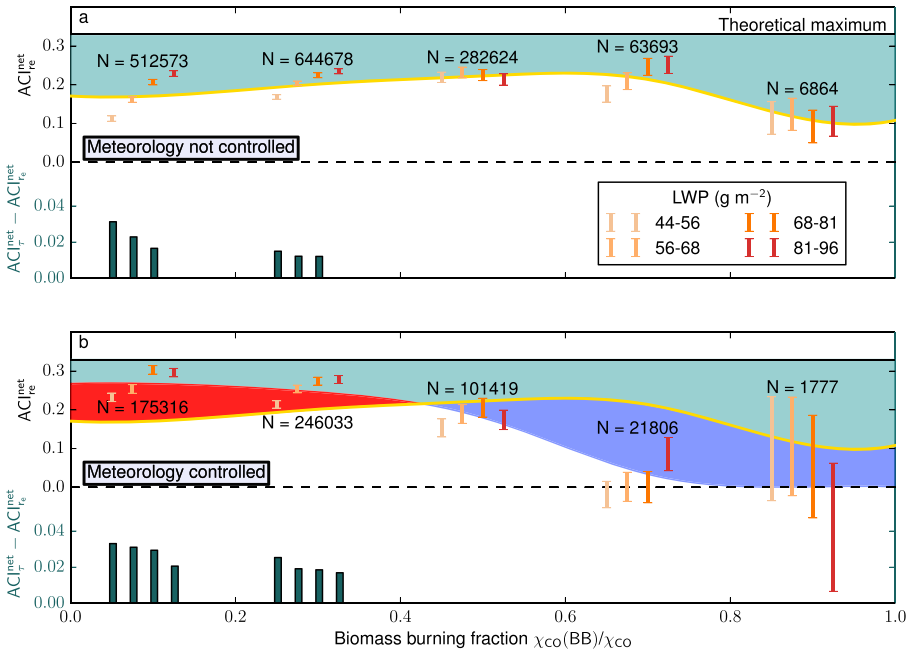

Figure 4. $ACI^{net}_{r_e}$ (a) as function of biomass-burning fraction $\chi_{CO}(BB)/\chi_{CO}$, LWP, and (b) whether the data set is limited to a narrow range of LTS and SH with T_C between −7.8°C and 4.8°C. Error bars indicate 95% confidence ranges for the calculated value of ACI^{net}. *N* indicates the number of equal area grid cells containing clouds that went into the calculation of the ACI^{net} parameter for the combined four LWP bins. $ACI^{net}_{\tau} - ACI^{net}_{r_e}$ is shown only when the difference between the two values is statistically significant (Text S4). The light blue area bounded by the yellow line represents the difference between the $ACI^{net}_{r_e}$ averaged over the four LWP bins and a theoretical maximum value of 0.33. Red and blue areas represent the calculated increase and decrease, respectively, in $ACI^{net}_{r_e}$ that is due to controlling for meteorology.

ANT plumes. Polluted BB aerosol regimes are associated with relatively high LTS, SH, and T_C compared to clean aerosol regimes; the opposite is observed for ANT aerosol regimes.

The implication is that observations of a possible covariance between clouds and aerosols can sometimes be more directly explained by a correlation of CO with meteorology. To assess the impact of pollution on clouds more precisely, we now limit our analyses to 1,980,186 grid cells or 20% of the total data set lying within a range between −7.8°C and 4.8°C for T_C, between 16.5 K and 21.8 K for LTS, and between 2.0 g kg^{-1} and 4.0 g kg^{-1} for SH (see Text S2 from the supporting information). With the data set constrained in this manner, the correlation coefficient of χ_{CO} to meteorological conditions drops from −0.18 to −0.03 for LTS, from 0.28 to 0.09 for SH, and from 0.39 to 0.17 for T_C. Because aerosol-cloud interactions are normally also evaluated within a narrow range of LWP (Feingold et al., 2003) since $r_e \propto \tau$/LWP, we further stratify the data set into four LWP bins between 44 g m^{-2} and 96 g m^{-2}.

Figure 4 shows values of $ACI^{net}_{r_e}$ in each of the four LWP bins as a function of the relative fraction of BB pollution to total pollution $\chi_{CO}(BB)/\chi_{CO}(Tot)$ and whether the data set is controlled for meteorological variability. The ACI^{net} parameter is the linear fit of retrieved cloud microphysical parameters to model values of χ_{CO} between 2005 and 2010 for clouds north of 65° in latitude (for details and an example see Text S3 and Figure S1 from the supporting information). The ACI parameter is calculated from all grid cells that satisfy the aforementioned selection criteria for meteorological parameters and aerosol type.

Controlling for each of LTS, SH, LWP, and T_C, the number of cloudy grid cells in each LWP bin ranges from 331 to 565 for BB plumes (1,777 grid cells total) and from 40,705 to 47,610 for ANT plumes (175,316 grid cells total). The difference between $ACI^{net}_{r_e}$ and ACI^{net}_{τ} is shown when the two quantities are statistically different (see Text S4 from the supporting information for details). One concern is that the solar zenith angle is generally high in the Arctic, and this can lead to a negative bias in retrievals of the effective radius (Grosvenor & Wood, 2014). Higher latitudes also correspond with lower values of low-level χ_{CO} (not shown) implying a possible negative bias in the calculations of ACI^{net} presented here. That said, the calculations of ACI^{net} consider relative changes thereby limiting the impact of any absolute bias on our results. In general, $ACI^{net}_{r_e}$ and ACI^{net}_{τ}

are similar; differences between the two are statistically significant but do not exceed 12%. This indicates a weak sensitivity of LWP to pollution. When the data set is not limited to the narrow meteorological range, ACI^{net} is positive for both the BB and ANT-dominated aerosol regimes, although values of ACI^{net} in BB aerosol regimes are generally lower by approximately 60%.

When the data set is limited to the narrow meteorological range previously described, ACI^{net} associated with ANT aerosol regimes increases relative to when meteorological constraints are not applied. It is close to the theoretical maximum value of 0.33 with an average uncertainty of 0.02. Meanwhile, applying the same meteorological constraints, ACI^{net} for BB aerosol regimes drops to near zero and is associated with an average uncertainty of 0.23. $ACI^{net}_{r_e}$ values in the ANT aerosol regimes range from 0.23 to 0.30 with probability values for the correlation (p values) lower than 0.05 (not shown). Values of $ACI^{net}_{r_e}$ in BB aerosol regimes range from −0.10 to 0.10 with p values greater than 0.1. Thus, no statistically significant relationship between BB aerosol plumes and cloud properties is observed—a previously observed correlation between χ_{CO}(BB) and cloud microphysical parameters (Tietze et al., 2011; Zamora et al., 2016) appears better explained by a correlation with meteorology. In fact, the Pearson correlation coefficients between χ_{CO} in BB-dominated regimes and LTS (0.19), SH (0.31), and T_C (0.25) are higher than the correlation coefficient between χ_{CO} and τ (0.17). The correlation of τ with SH (0.25) is particularly high.

A limitation of our method is that it cannot provide an explanation for why precisely we observe a higher sensitivity of clouds to ANT aerosol plumes than to BB plumes. It may be that pyrogenic aerosols are not particularly effective CCN (Andreae & Rosenfeld, 2008) at the low supersaturations that might be expected for stable arctic stratus (Earle et al., 2011). BB air parcels are on average associated with higher CO concentrations than ANT air parcels. Andersen et al. (2016) have shown that the effect of aerosols on cloud properties is limited at high aerosol and cloud droplet number concentrations. Because the ACI parameter considers logarithmic rather than linear changes in pollution and cloud properties, the differences in cloud sensitivities between ANT and BB plumes cannot be solely accounted for by differences in aerosol concentrations. Due to their hygroscopicity, freshly emitted BB plumes do not contain efficient CCN (Martin et al., 2013) and the meteorological conditions associated are not favorable for cloud formation (Fromm, 2005). En route to the Arctic, the aging of aerosols changes their properties (Konovalov et al., 2017; Li et al., 2003) and BB aerosols can become efficient CCN (Bougiatioti et al., 2016; Martin et al., 2013) that are particularly subject to precipitation due to their comparatively large size (Pósfai et al., 2003; Sakamoto et al., 2016). Concentrations of CO within BB plumes tend to correlate with moisture (Table 1). Given that precipitation decreases the correlation between CO and aerosols during long-range transport (Garrett et al., 2011), it may therefore be responsible for any observed difference between ACI values obtained in previous studies and the ACI^{net} values presented here. In any case, as shown by Table 1, interactions between BB plumes and clouds tend to be very rare.

An interesting result shown in Figure 4 is that ACI^{net} increases with LWP. This result for the Arctic contrasts with what has been presented for midlatitudes (Kim et al., 2008; McComiskey et al., 2009). With respect to LTS, Klein and Hartmann (1993) have shown that the formation of arctic cloud is more favorable under unstable environments, whereas the formation of midlatitude clouds is more favorable under stable environments. Similarly, Coopman et al. (2016) have shown that in the Arctic, ACI^{net} is greater under stable environments whereas the opposite is observed in midlatitudes (Andersen & Cermak, 2015; Chen et al., 2014). There appears to be fundamental differences between how arctic and midlatitude clouds respond to meteorology and aerosols.

5. Conclusions

An increasing number of studies are attempting to examine aerosol-cloud interactions while controlling for meteorological parameters (e.g., Chen et al., 2012, 2014; Christensen & Stephens, 2011; Lebsock et al., 2008; L'Ecuyer et al., 2009; Matsui et al., 2006), but only a few have focused on the Arctic (Tietze et al., 2011; Coopman et al., 2016). In terms of combined spatial and temporal coverage in the Arctic, and constraints made for meteorological variability, this study is perhaps the most comprehensive to date. Here we looked at the sensitivity ACI^{net} of arctic clouds to passive pollution plumes from distant sources rather than the sensitivity to local aerosols ACI. Precipitation can remove aerosols during long-range transport (Garrett et al., 2011) and therefore decrease the value of ACI^{net} relative to ACI. We find that observed values of ACI^{net} for anthropogenic pollution plumes already lie close to a theoretical maximum value of 0.33, implying that values of ACI are either similar or not significantly higher. Notably, ACI values derived using satellite observations from subpolar regions

range between 0.04 and 0.17 (Nakajima et al., 2001; Quaas et al., 2006) which is 2 to 8 times lower than ACI values described here. It appears that arctic clouds are more susceptible to pollution plumes than other regions. This result cannot be explained by generally low concentrations of aerosols in the region (Andersen et al., 2016) because the ACI^{net} calculation implicitly considers relative changes in pollution loading. It is possible that values of ACI are particularly high in the Arctic due to elevated LTS and a reduced potential for vertical mixing with subsaturated air. In less stable midlatitude regions, mixing processes decrease the sensitivity of clouds to aerosols by enhancing droplet evaporation (Kim et al., 2008).

Regardless of the precise mechanisms, the implication of the measurements is that arctic climate may be particularly sensitive to any future changes in anthropogenic pollution concentrations. Determining the effect of aerosol-cloud interactions on surface temperatures is complicated by the unique physics of the region: increasing τ not only brightens clouds but can also lead to a higher longwave cloud emissivity (Garrett & Zhao, 2006); either a significant net warming or cooling occurs depending on τ, the season, and the coverage of sea ice (Zhao & Garrett, 2015). In the future, a combination of reductions in emissions of midlatitude pollutants and increased wet scavenging in a warmer climate is anticipated to reduce the arctic aerosol burden by 61.0% by the end of the century (Klimont et al., 2013). Based on the ACI values found here, this can be expected to correspond to an 18% decrease in τ but with a possible compensating increase due to increasing arctic maritime transportation and industrialization (Peters et al., 2011). A further consideration is that the dynamic response of cloud amount to aerosols is itself a function of aerosols and meteorological conditions (Chen et al., 2014; Garrett et al., 2009). The ultimate climate impact remains to be determined.

Acknowledgments
We thank three anonymmous reviewers for constructive comments on the document. ERA-Interim data can be downloaded from the website: http://www.ecmwf.int/en/research/climate-reanalysis/era-interim. MODIS and POLDER-3 data sets can be downloaded from ICARE: http://www.icare.univ-lille1.fr/archive?dir=PARASOL/PM-L2/. The source code for the model used in this study, GEOS-Chem v9-01-03, is freely available at http://acmg.seas.harvard.edu/geos/. The setup used is available at http://wiki.seas.harvard.edu/geos-chem/index.php/Tagged_CO_simulation. This paper is dedicated posthumously to Kyle Tietze, who developed many of the techniques used in this study while a graduate student at the University of Utah. This material is based upon work supported by the National Science Foundation under grant 1303965, NERC studentship NE/K500835/1, the Pollution in the ARCtic System (PARCS) project (CNRS/INSU), and Université de Lille. The authors thank ICARE/AERIS, NASA, and CNES for the data used in this research.

References

Andersen, H., & Cermak, J. (2015). How thermodynamic environments control stratocumulus microphysics and interactions with aerosols. *Environmental Research Letters*, *10*(2), 024004. https://doi.org/10.1088/1748-9326/10/2/ 024004

Andersen, H., Cermak, J., Fuchs, J., & Schwarz, K. (2016). Global observations of cloud-sensitive aerosol loadings in low-level marine clouds. *Journal of Geophysical Research: Atmospheres*, *121*, 12,936–12,946. https://doi.org/10.1002/2016JD025614

Andreae, M., & Rosenfeld, D. (2008). Aerosol-cloud-precipitation interactions. Part 1. The nature and sources of cloud-active aerosols. *Earth-Science Reviews*, *89*(1-2), 13–41. https://doi.org/10.1016/j.earscirev.2008.03.001

Avey, L., Garrett, T. J., & Stohl, A. (2007). Evaluation of the aerosol indirect effect using satellite, tracer transport model, and aircraft data from the International Consortium for Atmospheric Research on Transport and Transformation. *Journal of Geophysical Research*, *112*, D10S33. https://doi.org/10.1029/2006JD007581

Baum, B. A., Menzel, W. P., Frey, R. A., Tobin, D. C., Holz, R. E., Ackerman, S. A., … Yang, P. (2012). MODIS cloud-top property refinements for collection 6. *Journal of Applied Meteorology and Climatology*, *51*(6), 1145–1163. https://doi.org/10.1175/JAMC-D-11-0203.1

Berrisford, P., Dee, D., Fielding, K., Fuentes, M., Kallberg, P., Kobayashi, S., & Uppala, S. (2011). The ERA-Interim Archive version 2.0 (Tech. Rep.) Reading, UK: ECMWF.

Bey, I., Jacob, D. J., Yantosca, R. M., Logan, J. a., Field, B. D., Fiore, A. M., … Schultz, M. G. (2001). Global modeling of tropospheric chemistry with assimilated meteorology: Model description and evaluation. *Journal of Geophysical Research*, *106*, 23,073–23,095. https://doi.org/10.1029/2001JD000807

Bougiatioti, A., Bezantakos, S., Stavroulas, I., Kalivitis, N., Kokkalis, P., Biskos, G., … Nenes, A. (2016). Biomass-burning impact on CCN number, hygroscopicity and cloud formation during summertime in the eastern Mediterranean. *Atmospheric Chemistry and Physics*, *16*(11), 7389–7409. https://doi.org/10.5194/acp-16-7389-2016

Bréon, F.-M., & Colzy, S. (1999). Cloud detection from the spaceborne polder instrument and validation against surface synoptic observations. *Journal of Applied Meteorology*, *38*(6), 777–785. https://doi.org/10.1175/1520-0450(1999)038<0777:CDFTSP>2.0.CO;2

Bréon, F.-M., Tanré, D., & Generoso, S. (2002). Aerosol effect on cloud droplet size monitored from satellite. *Science*, *295*(5556), 834–838. https://doi.org/10.1126/science.1066434

Brioude, J., Cooper, O. R., Feingold, G., Trainer, M., Freitas, S. R., Kowal, D., … Hsie, E.-Y. (2009). Effect of biomass burning on marine stratocumulus clouds off the California coast. *Atmospheric Chemistry and Physics*, *9*(22), 8841–8856. https://doi.org/10.5194/acp-9-8841-2009

Buriez, J. C., Vanbauce, C., Parol, F., Goloub, P., Herman, M., Bonnel, B., … Seze, G. (1997). Cloud detection and derivation of cloud properties from POLDER. *International Journal of Remote Sensing*, *18*(13), 2785–2813. https://doi.org/10.1080/014311697217332

Chen, Y.-C., Christensen, M. W., Stephens, G. L., & Seinfeld, J. H. (2014). Satellite-based estimate of global aerosol-cloud radiative forcing by marine warm clouds. *Nature Geoscience*, *7*(9), 643–646. https://doi.org/10.1038/ngeo2214

Chen, Y.-C., Christensen, M. W., Xue, L., Sorooshian, A., Stephens, G. L., Rasmussen, R. M., & Seinfeld, J. H. (2012). Occurrence of lower cloud albedo in ship tracks. *Atmospheric Chemistry and Physics*, *12*(17), 8223–8235. https://doi.org/10.5194/acp-12-8223-2012

Christensen, M. W., & Stephens, G. L. (2011). Microphysical and macrophysical responses of marine stratocumulus polluted by underlying ships: Evidence of cloud deepening. *Journal of Geophysical Research*, *116*, D03201. https://doi.org/10.1029/2010JD014638

Coopman, Q., Garrett, T. J., Riedi, J., Eckhardt, S., & Stohl, A. (2016). Effects of long-range aerosol transport on the microphysical properties of low-level liquid clouds in the Arctic. *Atmospheric Chemistry and Physics*, *16*(7), 4661–4674. https://doi.org/10.5194/acp-16-4661-2016

Cox, C. J., Walden, V. P., Rowe, P. M., & Shupe, M. D. (2015). Humidity trends imply increased sensitivity to clouds in a warming Arctic. *Nature Communications*, *6*(10), 117. https://doi.org/10.1038/ncomms10117

Dee, D. P., Uppala, S. M., Simmons, a. J., Berrisford, P., Poli, P., Kobayashi, S., … Vitart, F. (2011). The ERA-Interim reanalysis: Configuration and performance of the data assimilation system. *Quarterly Journal of the Royal Meteorological Society*, *137*(656), 553–597. https://doi.org/10.1002/qj.828

Earle, M. E., Liu, P. S. K., Strapp, J. W., Zelenyuk, A., Imre, D., McFarquhar, G. M., … Leaitch, W. R. (2011). Factors influencing the microphysics and radiative properties of liquid-dominated Arctic clouds: Insight from observations of aerosol and clouds during ISDAC. *Journal of Geophysical Research*, *116*, D00T09. https://doi.org/10.1029/2011JD015887

Feingold, G., Eberhard, W. L., Veron, D. E., & Previdi, M. (2003). First measurements of the Twomey indirect effect using ground-based remote sensors. *Geophysical Research Letters*, *30*, 1287. https://doi.org/10.1029/2002GL016633

Feingold, G., Remer, L. a., Ramaprasad, J., & Kaufman, Y. J. (2001). Analysis of smoke impact on clouds in Brazilian biomass burning regions: An extension of Twomey's approach. *Journal of Geophysical Research*, *106*(D19), 22,907–22,922. https://doi.org/10.1029/2001JD000732

Finch, D. P., Palmer, P. I., & Parrington, M. (2014). Origin, variability and age of biomass burning plumes intercepted during BORTAS-B. *Atmospheric Chemistry and Physics*, *14*(24), 13,789–13,800. https://doi.org/10.5194/ acp-14-13789-2014

Fisher, J. A., Jacob, D. J., Purdy, M. T., Kopacz, M., Le Sager, P., Carouge, C., … Wu, S. (2010). Source attribution and interannual variability of Arctic pollution in spring constrained by aircraft (ARCTAS, ARCPAC) and satellite (AIRS) observations of carbon monoxide. *Atmospheric Chemistry and Physics*, *10*(3), 977–996. https://doi.org/10.5194/acp-10-977-2010

Flannigan, M. D., Krawchuk, M. A., de Groot, W. J., Wotton, B. M., & Gowman, L. M. (2009). Implications of changing climate for global wildland fire. *International Journal of Wildland Fire*, *18*(5), 483. https://doi.org/10.1071/WF08187

Fromm, M. (2005). Pyro-cumulonimbus injection of smoke to the stratosphere: Observations and impact of a super blowup in northwestern Canada on 3–4 August 1998. *Journal of Geophysical Research*, *110*, D08205. https://doi.org/10.1029/2004JD005350

Garrett, T. J., & Zhao, C. (2006). Increased Arctic cloud longwave emissivity associated with pollution from mid-latitudes. *Nature*, *440*(7085), 787–789. https://doi.org/10.1038/nature04636

Garrett, T., Zhao, C., & Novelli, P. (2010). Assessing the relative contributions of transport efficiency and scavenging to seasonal variability in Arctic aerosol. *Tellus B: Chemical and Physical Meteorology*, *62*(3), 190–196. https://doi.org/10.1111/j.1600-0889.2010.00453.x

Garrett, T. J., Avey, L., Palmer, P. I., Stohl, A., Neuman, J. A., Brock, C. A., … Holloway, J. S. (2006). Quantifying wet scavenging processes in aircraft observations of nitric acid and cloud condensation nuclei. *Journal of Geophysical Research*, *111*, D23S51. https://doi.org/10.1029/2006JD007416

Garrett, T. J., Brattström, S., Sharma, S., Worthy, D. E. J., & Novelli, P. (2011). The role of scavenging in the seasonal transport of black carbon and sulfate to the Arctic. *Geophysical Research Letters*, *38*, L16805. https://doi.org/10.1029/2011GL048221

Garrett, T. J., Maestas, M. M., Krueger, S. K., & Schmidt, C. T. (2009). Acceleration by aerosol of a radiative-thermodynamic cloud feedback influencing Arctic surface warming. *Geophysical Research Letters*, *36*, L19804. https://doi.org/10.1029/2009GL040195

Grosvenor, D. P., & Wood, R. (2014). The effect of solar zenith angle on MODIS cloud optical and microphysical retrievals within marine liquid water clouds. *Atmospheric Chemistry and Physics*, *14*(14), 7291–7321. https://doi.org/10.5194/acp-14-7291-2014

Hirdman, D., Burkhart, J. F., Sodemann, H., Eckhardt, S., Jefferson, A., Quinn, P. K., … Stohl, A. (2010). Long-term trends of black carbon and sulphate aerosol in the Arctic: Changes in atmospheric transport and source region emissions. *Atmospheric Chemistry and Physics*, *10*(19), 9351–9368. https://doi.org/10.5194/acp-10-9351-2010

Kim, B.-G., Miller, M. a., Schwartz, S. E., Liu, Y., & Min, Q. (2008). The role of adiabaticity in the aerosol first indirect effect. *Journal of Geophysical Research*, *113*, D05210. https://doi.org/10.1029/2007JD008961

King, M. D., Platnick, S., Hubanks, P. A., Thomas Arnold, G., Moody, E. G., Wind, G., & Wind, B. (2006). Collection 005 change summary for the MODIS cloud optical property (06 _ OD) algorithm (Tech. Rep. MODIS Atmos.). NASA.

Klein, S. A., & Hartmann, D. L. (1993). The seasonal cycle of low stratiform clouds. *Journal of Climate*, *6*(8), 1587–1606. https://doi.org/10.1175/1520-0442(1993)006<1587:TSCOLS>2.0.CO;2

Klimont, Z., Smith, S. J., & Cofala, J. (2013). The last decade of global anthropogenic sulfur dioxide: 2000–2011 emissions. *Environmental Research Letters*, *8*(1), 014003. https://doi.org/10.1088/1748-9326/8/1/014003

Konovalov, I. B., Beekmann, M., Berezin, E. V., Formenti, P., & Andreae, M. O. (2017). Probing into the aging dynamics of biomass burning aerosol by using satellite measurements of aerosol optical depth and carbon monoxide. *Atmospheric Chemistry and Physics*, *17*(7), 4513–4537. https://doi.org/10.5194/acp-17-4513-2017

Lebsock, M. D., Stephens, G. L., & Kummerow, C. (2008). Multisensor satellite observations of aerosol effects on warm clouds. *Journal of Geophysical Research*, *113*, D15205. https://doi.org/10.1029/2008JD009876

L'Ecuyer, T. S., Berg, W., Haynes, J., Lebsock, M., & Takemura, T. (2009). Global observations of aerosol impacts on precipitation occurrence in warm maritime clouds. *Journal of Geophysical Research*, *114*, D09211. https://doi.org/10.1029/2008JD011273

Li, J., Pósfai, M., Hobbs, P. V., & Buseck, P. R. (2003). Individual aerosol particles from biomass burning in southern Africa: 2. Compositions and aging of inorganic particles. *Journal of Geophysical Research*, *108*(D13), 8484. https://doi.org/10.1029/2002JD002310

Lindholt, L., & Glomsrød, S. (2012). The Arctic: No big bonanza for the global petroleum industry. *Energy Economics*, *34*(5), 1465–1474. https://doi.org/10.1016/j.eneco.2012.06.020

Longley, I., Inglis, D., Gallagher, M., Williams, P., Allan, J., & Coe, H. (2005). Using NO_x and CO monitoring data to indicate fine aerosol number concentrations and emission factors in three UK conurbations. *Atmospheric Environment*, *39*(28), 5157–5169. https://doi.org/10.1016/j.atmosenv.2005.05.017

Mackie, A. R., Palmer, P. I., Barlow, J. M., Finch, D. P., Novelli, P., & Jaeglé, L. (2016). Reduced Arctic air pollution due to decreasing European and North American emissions. *Journal of Geophysical Research: Atmospheres*, *121*, 8692–8700. https://doi.org/10.1002/2016JD024923

Martin, M., Tritscher, T., Jurányi, Z., Heringa, M. F., Sierau, B., Weingartner, E., … Lohmann, U. (2013). Hygroscopic properties of fresh and aged wood burning particles. *Journal of Aerosol Science*, *56*, 15–29. https://doi.org/10.1016/j.jaerosci.2012.08.006

Matsui, T., Masunaga, H., Kreidenweis, S. M., Pielke, R. a., Tao, W.-K., Chin, M., & Kaufman, Y. J. (2006). Satellite-based assessment of marine low cloud variability associated with aerosol, atmospheric stability, and the diurnal cycle. *Journal of Geophysical Research*, *111*, D17204. https://doi.org/10.1029/2005JD006097

McComiskey, A., & Feingold, G. (2012). The scale problem in quantifying aerosol indirect effects. *Atmospheric Chemistry and Physics*, *12*(2), 1031–1049. https://doi.org/10.5194/acp-12-1031-2012

McComiskey, A., Feingold, G., Frisch, A. S., Turner, D. D., Miller, M. A., Chiu, J. C., … Ogren, J. A. (2009). An assessment of aerosol-cloud interactions in marine stratus clouds based on surface remote sensing. *Journal of Geophysical Research*, *114*, D09203. https://doi.org/10.1029/2008JD011006

Monks, S. A., Arnold, S. R., & Chipperfield, M. P. (2012). Evidence for El Niño–Southern Oscillation (ENSO) influence on Arctic CO interannual variability through biomass burning emissions. *Geophysical Research Letters*, *39*, L14804. https://doi.org/10.1029/2012GL052512

Nakajima, T., Higurashi, A., Kawamoto, K., & Penner, J. E. (2001). A possible correlation between satellite-derived cloud and aerosol microphysical parameters. *Geophysical Research Letters*, *28*(7), 1171–1174. https://doi.org/10.1029/2000GL012186

Paris, J.-D., Stohl, A., Nédélec, P., Arshinov, M. Y., Panchenko, M. V., Shmargunov, V. P., … Ciais, P. (2009). Wildfire smoke in the Siberian Arctic in summer: Source characterization and plume evolution from airborne measurements. *Atmospheric Chemistry and Physics*, *9*(23), 9315–9327. https://doi.org/10.5194/acp-9-9315-2009

Parrington, M., Palmer, P. I., Henze, D. K., Tarasick, D. W., Hyer, E. J., Owen, R. C., … Worden, J. R. (2012). The influence of boreal biomass burning emissions on the distribution of tropospheric ozone over North America and the North Atlantic during 2010. *Atmospheric Chemistry and Physics*, *12*(4), 2077–2098. https://doi.org/10.5194/acp-12-2077-2012

Peters, G. P., Nilssen, T. B., Lindholt, L., Eide, M. S., Glomsrød, S., Eide, L. I., & Fuglestvedt, J. S. (2011). Future emissions from shipping and petroleum activities in the Arctic. *Atmospheric Chemistry and Physics*, *11*(11), 5305–5320. https://doi.org/10.5194/acp-11-5305-2011

Pizzolato, L., Howell, S. E. L., Derksen, C., Dawson, J., & Copland, L. (2014). Changing sea ice conditions and marine transportation activity in Canadian Arctic waters between 1990 and 2012. *Climatic Change*, *123*(2), 161–173. https://doi.org/10.1007/s10584-013-1038-3

Platnick, S., King, M., Ackerman, S., Menzel, W., Baum, B., Riedi, J., & Frey, R. (2003). The MODIS cloud products: Algorithms and examples from terra. *IEEE Transactions on Geoscience and Remote Sensing*, *41*(2), 459–473. https://doi.org/10.1109/TGRS.2002.808301

Pósfai, M., Simonics, R., Li, J., Hobbs, P. V., & Buseck, P. R. (2003). Individual aerosol particles from biomass burning in southern Africa: 1. Compositions and size distributions of carbonaceous particles. *Journal of Geophysical Research*, *108*(D13), 8483. https://doi.org/10.1029/2002JD002291

Quaas, J., Boucher, O., & Lohmann, U. (2006). Constraining the total aerosol indirect effect in the LMDZ and ECHAM4 GCMs using MODIS satellite data. *Atmospheric Chemistry and Physics*, *6*(4), 947–955. https://doi.org/10.5194/acp-6-947-2006

Riedi, J., Marchant, B., Platnick, S., Baum, B. A., Thieuleux, F., Oudard, C., … Dubuisson, P. (2010). Cloud thermodynamic phase inferred from merged POLDER and MODIS data. *Atmospheric Chemistry and Physics*, *10*(23), 11,851–11,865. https://doi.org/10.5194/acp-10-11851-2010

Sakamoto, K. M., Laing, J. R., Stevens, R. G., Jaffe, D. A., & Pierce, J. R. (2016). The evolution of biomass-burning aerosol size distributions due to coagulation: Dependence on fire and meteorological details and parameterization. *Atmospheric Chemistry and Physics*, *16*(12), 7709–7724. https://doi.org/10.5194/acp-16-7709-2016

Stevens, B., & Feingold, G. (2009). Untangling aerosol effects on clouds and precipitation in a buffered system. *Nature*, *461*(7264), 607–613. https://doi.org/10.1038/nature08281

Stephens, G. L., Vane, D. G., Boain, R. J., Mace, G. G., Sassen, K., Wang, Z., … CloudSat Science Team (2002). The CloudSat mission anf the A-Train. *Bulletin of the American Meteorological Society*, *83*(12), 1771–1790. https://doi.org/10.1175/BAMS-83-12-1771

Stohl, A. (2006). Characteristics of atmospheric transport into the Arctic troposphere. *Journal of Geophysical Research*, *111*, D11306. https://doi.org/10.1029/2005JD006888

Stohl, a., Berg, T., Burkhart, J. F., Fjæraa, A. M., Forster, C., Herber, A., … Yttri, K. E. (2007). Arctic smoke—record high air pollution levels in the European Arctic due to agricultural fires in Eastern Europe in spring 2006. *Atmospheric Chemistry and Physics*, *7*(2), 511–534. https://doi.org/10.5194/acp-7-511-2007

Tietze, K., Riedi, J., Stohl, A., & Garrett, T. J. (2011). Space-based evaluation of interactions between aerosols and low-level Arctic clouds during the Spring and Summer of 2008. *Atmospheric Chemistry and Physics*, *11*(7), 3359–3373. https://doi.org/10.5194/acp-11-3359-2011

Warneke, C., Bahreini, R., Brioude, J., Brock, C. a., de Gouw, J. A., Fahey, D. W., … Veres, P. (2009). Biomass burning in Siberia and Kazakhstan as an important source for haze over the Alaskan Arctic in April 2008. *Geophysical Research Letters*, *36*, L02813. https://doi.org/10.1029/2008GL036194

Warneke, C., Froyd, K. D., Brioude, J., Bahreini, R., Brock, C. A., Cozic, J., … Stohl, A. (2010). An important contribution to springtime Arctic aerosol from biomass burning in Russia. *Geophysical Research Letters*, *37*, L01801. https://doi.org/10.1029/2009GL041816

Yang, Q., Easter, R. C., Campuzano-Jost, P., Jimenez, J. L., Fast, J. D., Ghan, S. J., … Wisthaler, A. (2015). Aerosol transport and wet scavenging in deep convective clouds: A case study and model evaluation using a multiple passive tracer analysis approach. *Journal of Geophysical Research: Atmospheres*, *120*, 8448–8468. https://doi.org/10.1002/2015JD023647

Zamora, L. M., Kahn, R. a., Cubison, M. J., Diskin, G. S., Jimenez, J. L., Kondo, Y., … Ziemba, L. D. (2016). Aircraft-measured indirect cloud effects from biomass burning smoke in the Arctic and subarctic. *Atmospheric Chemistry and Physics*, *16*(2), 715–738. https://doi.org/10.5194/acp-16-715-2016

Zhao, C., & Garrett, T. J. (2015). Effects of Arctic haze on surface cloud radiative forcing. *Geophysical Research Letters*, *42*, 557–564. https://doi.org/10.1002/2014GL062015